INTERNATIONAL JOURNAL OF OPTIMIZATION IN CIVIL ENGINEERING
Int. J. Optim. Civil Eng., 2021; 11(2):155-176

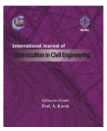

SEISMIC OPTIMIZATION OF STEEL MOMENT RESISTING FRAMES CONSIDERING SOIL-STRUCTURE INTERACTION

A. Milany and S. Gholizadeh[*, †]
Department of Civil Engineering, Urmia University, Urmia, Iran

ABSTRACT

The main purpose of the present work is to investigate the impact of soil-structure interaction on performance-based design optimization of steel moment resisting frame (MRF) structures. To this end, the seismic performance of optimally designed MRFs with rigid supports is compared with that of the optimal designs with a flexible base in the context of performance-based design. Two efficient metaheuristic algorithms, namely center of mass optimization and improved fireworks, are used to implement the optimization task. During the optimization process, nonlinear structural response-history analysis is carried out to evaluate the structural response. Two illustrative design examples of 6- and 12-story steel MRFs are presented, and it is observed that the performance-based design optimization considering soil-structure interaction decreases the structural weight and increases nonlinear structural response in comparison to rigid-based models. Therefore, in order to obtain more realistic optimal designs, soil-structure interaction should be included in the performance-based design optimization process of steel MRFs.

Keywords: performance-based design; soil-structure interaction; structural optimization; steel moment resisting frame; metaheuristic.

Received: 5 January 2021; Accepted: 10 May 2021

1. INTRODUCTION

In the last recent years, performance-based design (PBD) optimization of structures has become a popular topic in the field of structural engineering. During the PBD optimization process, the seismic response of structures can be evaluated by static or dynamic nonlinear structural analyses. It is clear that the dynamic response of structures may be seriously affected by the soil–structure interaction (SSI) [1, 2]. In most studies on the seismic design and performance evaluation of steel moment-resisting frame (MRF) structures, the supports

[*]Corresponding author: Department of Civil Engineering, Urmia University, Urmia, P.O. box 165, Iran
[†]E-mail address: s.gholizadeh@urmia.ac.ir (S. Gholizadeh)

have been considered as fixed [3-18] however, several studies have been conducted to investigate the effects of SSI on the seismic behavior of steel MRFs. Nakhaei and Ghannad [19] studied the effects of SSI on the Park-Ang damage index using Cone method. Sáez et al. [20] investigated the inelastic soil effects on the seismic vulnerability of steel MRFs using nonlinear dynamic analysis. Raychowdhury [21] has studied the dynamic SSI effects on the seismic performance of a steel MRFs based on beam-on-nonlinear-Winkler-foundation (BNWF) model. Ganjavi and Hao [22] conducted a parametric study on the effect of SSI on the lateral load distribution pattern based on Cone method. Sáez et al. [23] proposed a method for nonlinear soil modeling and dynamic analysis to evaluate the seismic performance of MRFs. Raychowdhury and Ray-Chaudhuri [24] studied the effect of SSI on the seismic behavior of non-structural components of steel MRFs utilizing BNWF model. The effects of SSI were assessed on the seismic behavior of shear buildings by Lu et al. [25] using a parametric study based on Cone method. Aydemir and Ekiz [26] addressed the seismic behavior of flexible base multi-story frames subjected to earthquake loading considering soil–structure interaction under earthquake excitation. Ghandil and Behnamfar [27] used the direct modeling method and studied the ductility of steel MRFs by defining soil as an equivalent linear approach for the near-field area. Farhadi et al. [28] proposed a method for estimating and converting the response of fixed-base steel MRFs to SSI-considered situation based on BNWF model. Ganjavi et al. [29] investigated the effects of SSI on the lateral load distribution pattern of steel MRFs employing Cone method. Mashhadi et al. [30] studied the effect of near-field earthquake and foundation safety factor on the seismic behavior of steel MRFs using the BNWF model for SSI. Jafarieh and Ghannad [31] parametrically investigated the effect of foundation uplift on the seismic behavior of structures considering SSI. Fathizadeh et al. [32] optimized steel MRF structures using a Winkler-based method to consider SSI effects.

The literature review reveals the sparsity of the literature on the coupling of PBD optimization and SSI effects for the seismic design of steel MRFs. On the other hand, the feasible optimum solutions are attained in such a way that the structural responses are less than and close to their allowable limits. Therefore, excluding the effects of SSI from the PBD optimization process can lead to a violation of the design constraints and obtaining infeasible designs. Accordingly, in this study, the effects of SSI are considered in the seismic PBD optimization process of steel MRFs. During the recent years, metaheuristics have been extensively used in different disciplines of structural engineering and a wide variety of metaheuristic algorithms has been proposed in literature. In the current study, two efficient metaheuristics namely, center of mass optimization (CMO) [33] and improved fireworks algorithm (IFWA) [34], are employed to tackle the PBD optimization problem of steel MRFs. The efficiency of CMO and IFWA for solving PBD optimization problems of steel structures has been demonstrated in [35].

Two illustrative examples of 6- and 12-story steel MRFs with and without SSI effects are presented and optimized in the framework of PBD using CMO and IFWA metaheuristics. the Nonlinear Winkler-based method is used to soil-foundation modeling and structural response is evaluated by performing nonlinear response history analysis. The numerical results demonstrate that for both 6- and 12-story steel MRFs, PBD optimization of the flexible base models, constructed by considering SSI, gives lighter structural weights compared to fixed base models.

2. STRUCTURAL SEISMIC DESIGN OPTIMIZATION

In the present work, a performance-based design (PBD) methodology is applied to design of steel MRF structures. In the PBD methodology, immediate occupancy (IO), life safety (LS) and collapse prevention (CP) performance levels are considered correspond to seismic hazard levels of 50%, 10%, and 2% probability of exceedance in 50 years, respectively. Nonlinear response history analysis (NRHA) is performed to evaluate seismic structural response of steel MRFs. The most important issues for performing NRHA are selecting and scaling ground motions, appropriate definition of the damping mechanism, and proper modeling of support condition. In this study, OpenSees is used to perform NRHA.

2.1 Ground motion records

Following the FEMA-P695 [36] record selection criteria, a total number of 16 far-field ground motions recorded on Stiff soil sites (Class D) are selected in this study. For performing NRHA of planar structures, the horizontal component related to the largest PGA has been selected as given in Table 1.

Table 1: Ground motion records set [36]

ID	Record No.	M	Year	Name	Recording Station	PGA_{max} (g)
12011	953	6.7	1994	Northridge	Beverly Hills - Mulhol	0.52
12012	960	6.7	1994	Northridge	Canyon Country-WLC	0.48
12041	1602	7.1	1999	Duzce, Turkey	Bolu	0.82
12061	169	6.5	1979	Imperial Valley	Delta	0.35
12062	174	6.5	1979	Imperial Valley	El Centro Array #11	0.38
12072	1116	6.9	1995	Kobe, Japan	Shin-Osaka	0.24
12081	1158	7.5	1999	Kocaeli, Turkey	Duzce	0.36
12091	900	7.3	1992	Landers	Yermo Fire Station	0.24
12092	848	7.3	1992	Landers	Coolwater	0.42
12101	752	6.9	1989	Loma Prieta	Capitola	0.53
12102	767	6.9	1989	Loma Prieta	Gilroy Array #3	0.56
12121	721	6.5	1987	Superstition Hills	El Centro Imp. Co.	0.36
12122	725	6.5	1987	Superstition Hills	Poe Road (temp)	0.45
12132	829	7.0	1992	Cape Mendocino	Rio Dell Overpass	0.55
12141	1244	7.6	1999	Chi-Chi, Taiwan	CHY101	0.44
12151	68	6.6	1971	San Fernando	LA - Hollywood Stor	0.21

For all the selected ground motions, 5%-damped acceleration response spectra of records are amplitude-scaled to the Iranian seismic code's design spectrum. According to the ASCE-41-13 [37], each ground motion shall be scaled in a way that the average of spectra from all records generally matches or exceeds the target response spectrum over the period range $0.2T$ to $1.5T$, in which T is the first-mode period in the principal horizontal direction of response. Therefore, record scaling is performed for each structure individually, and the period variability of systems directly affects their seismic spectral demands. It should be noted that the design spectrum of the Iranian seismic code belongs to the BSE-1 hazard level, corresponding to a 10% probability of exceedance in 50 years.

2.2 Nonlinear SSI model

Nonlinear Winkler-based modeling method with nonlinear soil modeling, which is in the category of sub-structure modeling approaches, is used to simulate the soil-foundation interaction under the structures. The Beam-on-Nonlinear Winkler Foundation (BNWF) model [38] has been developed and validated based on experiment results performed on square and strip foundations [38-40]. The results of previous studies have shown that the BNWF model has an excellent ability to estimate the behavior of surface foundations on clay and sand under a variety of loading types [41-44]. Due to the addition of this model's nonlinear materials to the OpenSees material library and the design of a "ShallowFoundationGen" command, the application of the BNWF model in OpenSees software is readily possible [43]. Soil modeling is achieved by assigning independent nonlinear elements that are closely spaced. These elements are constructed by combining of spring, damper, and gap elements.

In the BNWF model, three types of springs are defined, one type of vertical spring to restrain the rocking, uplift, and settlement of the foundation (q-z), and two types of horizontal springs to restrain the lateral movements of the foundation (p-x and t-x) in which the p-x spring is used to derive the passive lateral pressure of the soil and the t-x spring is used to obtain the friction of the foundation floor against sliding. The defined characteristics for the behavior of the materials used in this model were inherently determined by Boulanger et al. [44] in the case of pile foundations then, by calibrating these characteristics based on the results of experiments on surface footings, the specific material models were developed by Raychowdhury and Hutchinson [38]. The property of the materials defined for the q-z, p-x, and t-x springs in the OpenSees platform is named QzSimple2, PxSimple1, and TxSimple1, respectively, and their constitutive curves and distribution of the springs are illustrated in Fig. 1.

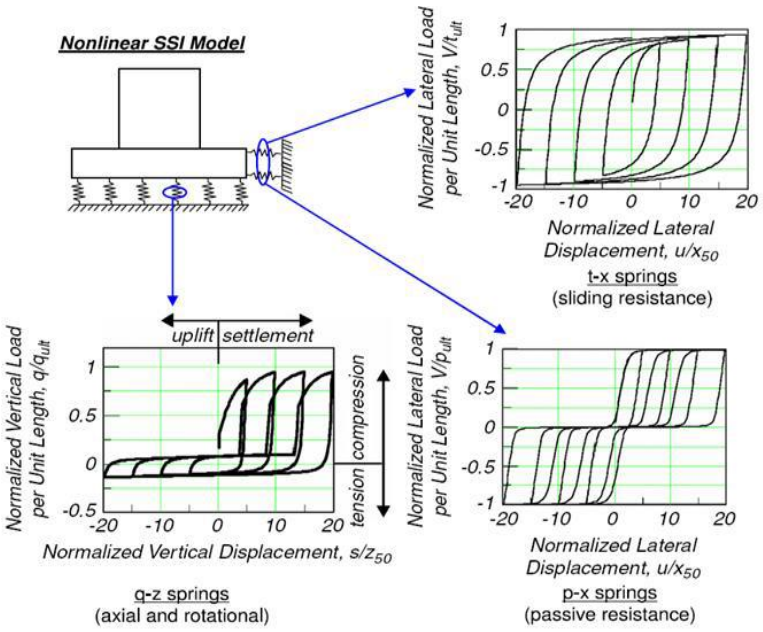

Figure 1. SSI model: Beam on Nonlinear Winkler-Foundation, Setup and Cyclic response [38]

Based on the observations of experimental results, it has been concluded that regarding the foundation rocking motion, to retain the stability of the structure, the compression zone springs at the end of the foundation should have a higher stiffness [40] therefore, as shown in Fig. 1, higher values are selected for the stiffness of the springs at the end of the foundation. In this paper, the number of vertical springs q-z is 23 (4.54% of the footing length), and the number of p-x and t-x springs is 1.

2.3 Objective function, variables and constraints

The objective function of the optimization problem is structural weight. Design variables are cross-sections of beams and columns of steel MRFs. Design constraints are geometric, strength (for gravity load combination), strong column-weak beam, and PBD constraints including confidence levels [46] at IO and CP levels and plastic rotation of structural elements [37] at IO, LS and CP levels. The formulation of the optimization problem is presented as follows:

Find: $$X = \left[x_1, x_2, \ldots, x_{ng} \right]^T \tag{1}$$

To minimize: $$W(X) = \sum_{i=1}^{ne} \rho_i . A_i . L_i \tag{2}$$

Subject to: $$g_i(X) \le 0, \quad i = 1,2,\ldots,nc \tag{3}$$

Geometric Const.: $$g_G(X) = \left(\frac{b_f^B}{b_f^{Cl}}, \frac{b_f^{Cu}}{b_f^{Cl}}, \frac{h^u}{h^l}, \frac{t_w^u}{t_w^l} \right) - 1 \tag{4}$$

Strength Const.: $$g_S(X) = \begin{cases} \frac{1}{2} . \frac{P_u}{\phi_c P_n} + \frac{M_u}{\phi_b M_n} - 1 & if \ \frac{P_u}{f_c P_n} < 0.2 \\ \frac{P_u}{\phi_c P_n} + \frac{8}{9} \frac{M_u}{\phi_b M_n} - 1 & if \ \frac{P_u}{\phi_c P_n} \ge 0.2 \end{cases} \tag{5}$$

SCWB Const.: $$g_W(X) = \frac{\sum M_{pb}}{\sum M_{pc}} - 1 \tag{6}$$

Drift Const.: $$g_D(X) = \frac{CL^i}{CL^i_{all}} - 1, \quad \begin{cases} i = IO, CP \\ CL^{IO}_{all} = 50\% \ , \ CL^{CP}_{all} = 90\% \end{cases} \tag{7}$$

Plastic Rot. Const.: $$g_P(X) = \frac{\theta^i_k}{\theta^i_{all}} - 1, \quad i = IO, CP; k = 1,2,\ldots,ne \tag{8}$$

where X is vector of design variables; W is the structural weight to be minimized under $g_i(X)$ constraints; ρ, A and L are weight density, cross-sectional area and length of structural element, respectively; ne is the number of elements; b_f, h, t_w are beam or column sections flange width, column sections total depth and column sections web thickness; P_u and M_u are the required axial and flexural strengths and $\phi_c P_n$ and $\phi_b M_n$ are factored nominal axial and flexural strengths, respectively; CL is the confidence level; and θ is plastic rotation of elements.

3. METAHEURISTIC ALGORITHMS

In this study, the Center of Mass Optimization (CMO) [33] and Improved Fireworks Algorithm (IFWA) [34] are used to deal with the PBD optimization problem of steel MRFs. In the following, the fundamental steps of these algorithms are described in brief.

3.1 CMO

CMO algorithm has been developed on the basis that the smaller the mass of search agents, the larger the distance to their center of mass and vice versa. The ability to switch between exploration and exploitation is one of the key features of this algorithm. The mechanism of moving and updating the position of particles in the CMO algorithm is as follows:

A controlling parameter (CP) is defined based on the following formula so that its maximum value in the first iteration is equal to 1.0 and minimum in the last iteration is equal to 0.0.

$$CP(t) = exp(-5t / t_{max}) \tag{9}$$

In each iteration t, the position of the center of mass and the distance of the particles are calculated based on the following equations:

$$X^C(t) = \frac{m_{g1}X_{g1}(t) + m_{g2}X_{g2}(t)}{m_{g1} + m_{g2}} \tag{10}$$

$$D(t) = \left|X_{g1}(t) - X_{g2}(t)\right| \tag{11}$$

in which X_{g1} and X_{g2} are particles in the first and second groups, respectively, and m_{g1} and m_{g2} are their corresponding masses.

In the exploration phase, the position of each particle is updated as follows:

$$if\ D_t > CP = \begin{cases} X_{g1}(t+1) = X_{g1}(t) - R_1(t).\left(X^C(t) - X_{g1}(t)\right) + R_2(t).\left(X_{best}(t) - X_{g1}(t)\right) \\ X_{g2}(t+1) = X_{g2}(t) + R_3(t).\left(X^C(t) - X_{g2}(t)\right) + R_4(t).\left(X_{best}(t) - X_{g2}(t)\right) \end{cases} \tag{12}$$

where R_1 to R_4 are vectors of random numbers in the range of [0,1] and X_{best} is the best solution.

After the exploration stage, in the final steps of the search process, to find a more accurate optimal response (exploitation), the position updating is achieved as follows in which R_5 and R_6 are random numbers in the range of [0, 1].

$$if\ D_t \le CP = \begin{cases} X_{g1}(t+1) = X_{g1}(t) + R_5(t).\left(X_{g1}(t) - X_{g2}(t)\right) \\ X_{g2}(t+1) = X_{g2}(t) + R_6(t).\left(X_{g1}(t) - X_{g2}(t)\right) \end{cases} \tag{13}$$

3.2 IFWA

Inspired by the fireworks event, The FWA algorithm has been designed as an optimization algorithm in the swarm intelligence category by simulating the search space to the spark explosion amplitude. Improved Fireworks Algorithm (IFWA) [34] is an efficient metaheuristic and searches the design space as follows:

In the first step, n fireworks are randomly distributed in the search space, and their fitness is calculated, then the best positions are selected as the next step fireworks.

The number of sparks and the explosion amplitude A_0 will be calculated for each firework in the next step. The explosion amplitude is initially calculated using the following equation and modified in the optimization process based on fitness of fireworks.

$$A_0 = 0.5\left(X_L + X_U\right) \tag{14}$$

Sparks are generated around each firework based on the following equation in which R_1 and R_2 are random values in the range of [− 1, +1] and $X(t)$ is the firework around which sparks are generated

$$\hat{X}\left(t+1\right) = X\left(t+1\right) + R_1\left(t\right).A\left(t\right) + R_2\left(t\right).\left(X\left(t+1\right) - X\left(t\right)\right) \tag{15}$$

After generating sparks and evaluating their fitness, if the value of the objective function in the spark position is better than the corresponding Firework, that spark is selected as Firework in the next step, and its explosion amplitude is adjusted according to the following equation. C_A is an amplification factor.

$$A\left(t+1\right) = C_A.A\left(t\right) \tag{16}$$

Otherwise, no spark will replace the relevant firework, and the fireworks explosion amplitude will be reduced to adjust the search more accurately in the next iteration with the C_R shrinkage factor as follows

$$A\left(t+1\right) = C_R.A\left(t\right) \tag{17}$$

It should be noted that C_A and C_R parameters are the most important parameters of the IFWA algorithm that are determined by sensitivity analysis.

4. NUMERICAL MODELING

In this study, the design optimization problem of steel special MRF structures is tackled with and without considering SSI effects. The NRHA is conducted to evaluate the structural seismic performance subjected to a suit of earthquake records given by FEMA-P695 [36]. To determine the scale factor for considered hazard levels, the amplitude scaling method is used following the design spectrum for the region of Iran. During the optimization process,

the sections of columns and beams are selected from the database of highly ductile W-shaped sections listed in Table 2.

Table 2: Database of steel sections for beams and columns

Beams				Columns			
No.	Profile	No.	Profile	No.	Profile	No.	Profile
1	W27×94	11	W16×57	1	W14×455	11	W14×193
2	W24×84	12	W18×46	2	W14×426	12	W14×176
3	W24×76	13	W16×50	3	W14×398	13	W14×159
4	W24×62	14	W16×40	4	W14×370	14	W14×145
5	W21×68	15	W16×45	5	W14×342	15	W14×132
6	W24×55	16	W18×35	6	W14×311	16	W14×82
7	W21×57	17	W12×50	7	W14×283	17	W14×74
8	W21×50	18	W12×35	8	W14×257	18	W14×68
9	W21×44	19	W12×22	9	W14×233	19	W14×53
10	W18×50	20	W12×19	10	W14×211	20	W14×48

The structural models of steel MRFs are constructed based on a centerline-to-centerline idealization and end zones are neglected. In addition, P-delta effects are considered in all analyses. The beams and columns are modeled by force-based beam-column fiber elements to represent the nonlinear behavior. The constitutive law is considered to be bilinear with pure kinematic strain hardening slope equal to 2% of the elastic modulus.

Two optimization processes are carried out for steel special MRFs with and without SSI effects and the results are compared in terms of optimal weight and inter-story drifts.

The statistical comparison of results obtained in this study is performed by using bar graphs to simplify the presentation. As shown in Fig. 2, the minimum, maximum, average, and standard deviation (SD) of a dataset are given in a bar graph.

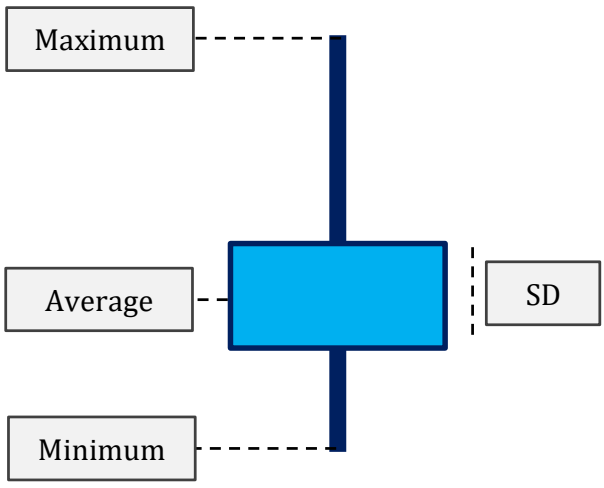

Figure 2. Bar graph

5. NUMERICAL EXAMPLES

Two illustrative examples of 6- and 12-story steel special MRFs are presented and their member grouping details are shown in Fig. 3. The dead and live loads of 3000 and 1200 kg/m are respectively applied to all beams. Steel material of ASTM A913 Gr. 50, with modulus of elasticity of 200 GPa and yield stress of 344 MPa is considered. For 6- and 12-story MRFs confidence levels of 50% and 90% correspond to 1.0673% and 5.9385% maximum inter-story drift at IO and CP performance levels, respectively.

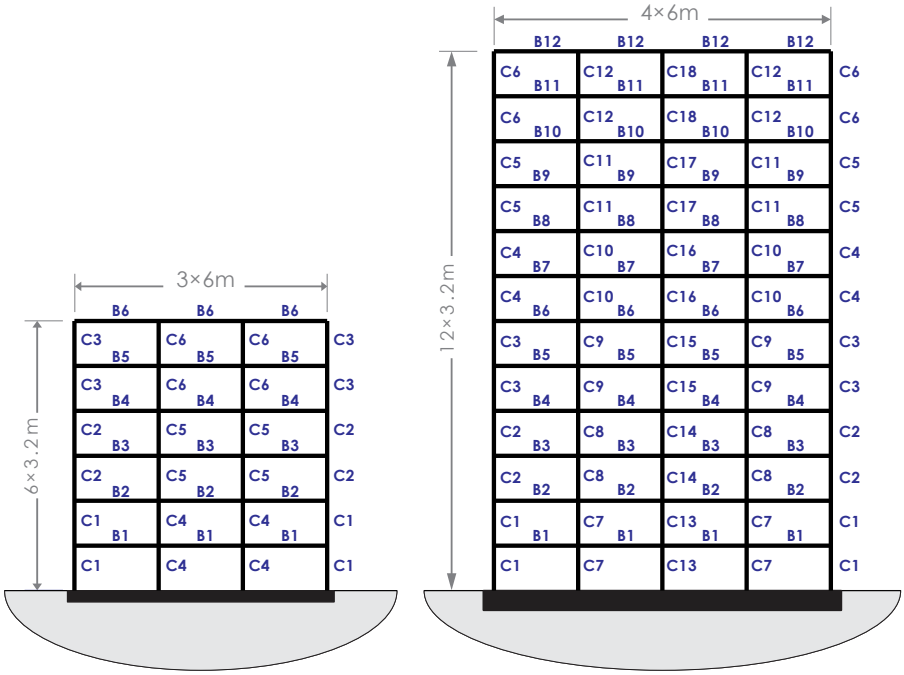

Figure 3. 6- and 12-story steel MRFs

In the case of each design example, two PBD optimization cases of fixed base and flexible base models are carried out by CMO and IFWA metaheuristics. In each optimization case, to account for the stochastic nature of the employed metaheuristics, 20 independent optimization runs are performed and fixed base and flexible base optimal designs are compared in terms of optimal weight (W) and maximum inter-story drift at IO and CP performance levels ($\delta_{\max}^{\mathrm{IO}}$ and $\delta_{\max}^{\mathrm{CP}}$). Furthermore, cross-sections of beams and columns of the optimal designs are given in Appendix.

5.1 6-story MRF

Using BNWF for soil-structure interaction modeling of 6-story structures, sandy soil with a unit weight of 18 kN/m^3 is considered, shear wave velocity is considered 185 m/s, cohesion is 5000 kPa and the friction angle is 38◦. The total length of the foundation is 18 m, the width of the strip related to the desired frame is 1.6 m and the height of the foundation is 0.8 m. The modeling parameters R_k, R_e, S_e are equal to 1.43, 0.06, 0.05, respectively. In this example, the number of particles and the maximum number of iterations are considered to

be 50 and 100, respectively. The results of 20 independent optimization runs are presented in Table 3. The comparison of the results is achieved using bar graphs shown in Fig. 4 and mean convergence history curves of the algorithms are depicted in Fig. 5.

Table 3: Results of independent optimization runs for fixed and flexible base 6-story MRFs

Design No.	Fixed base						Flexible base					
	IFWA			CMO			IFWA			CMO		
	W (kg)	δ_{max}^{IO} (%)	δ_{max}^{CP} (%)	W (kg)	δ_{max}^{IO} (%)	δ_{max}^{CP} (%)	W (kg)	δ_{max}^{IO} (%)	δ_{max}^{CP} (%)	W (kg)	δ_{max}^{IO} (%)	δ_{max}^{CP} (%)
1	14911	1.0440	3.0984	14435	1.0205	3.2616	14615	1.0639	2.9932	14066	1.0409	3.1002
2	14631	1.0460	2.9271	14426	1.0431	3.3683	**14160**	**1.0611**	**3.0864**	**13638**	**1.0520**	**3.0724**
3	15106	1.0637	3.0991	14691	1.0170	3.0648	14160	1.0611	3.0864	13638	1.0520	3.0724
4	15297	1.0318	3.0262	14708	1.0281	3.1742	14615	1.0639	2.9932	14066	1.0409	3.1002
5	14911	1.0440	3.0984	**14358**	**1.0583**	**3.0841**	14160	1.0611	3.0864	14066	1.0409	3.1002
6	15023	1.0436	3.2361	14483	1.0496	2.8944	14615	1.0639	2.9932	14615	1.0639	2.9932
7	14974	1.0454	2.9286	14435	1.0205	3.2616	14160	1.0611	3.0864	13638	1.0520	3.0724
8	14871	1.0285	3.1742	14631	1.0460	2.9271	14902	1.0329	3.2576	14160	1.0611	3.0864
9	14871	1.0285	3.1742	14691	1.0170	3.0648	14902	1.0329	3.2576	14066	1.0409	3.1002
10	14708	1.0281	3.1742	14691	1.0170	3.0648	14615	1.0639	2.9932	13638	1.0520	3.0724
11	14956	1.0360	3.0300	14631	1.0460	2.9271	14902	1.0329	3.2576	14239	1.0672	3.2455
12	**14631**	**1.0460**	**2.9271**	14631	1.0460	2.9271	14160	1.0611	3.0864	14239	1.0672	3.2455
13	14708	1.0281	3.1742	14631	1.0460	2.9271	14902	1.0329	3.2576	13638	1.0520	3.0724
14	14691	1.0170	3.0648	14631	1.0460	2.9271	14160	1.0611	3.0864	13638	1.0520	3.0724
15	14704	1.0441	3.2444	14631	1.0460	2.9271	14160	1.0611	3.0864	13638	1.0520	3.0724
16	15073	1.0621	3.0956	14483	1.0496	2.8944	14615	1.0639	2.9932	14615	1.0639	2.9932
17	14956	1.0360	3.0300	14708	1.0281	3.1742	14902	1.0329	3.2576	14160	1.0611	3.0864
18	14631	1.0460	2.9271	14426	1.0431	3.3683	14160	1.0611	3.0864	14239	1.0672	3.2455
19	15304	1.0235	2.9694	14631	1.0460	2.9271	14239	1.0672	3.2455	14160	1.0611	3.0864
20	14631	1.0460	2.9271	14631	1.0460	2.9271	14902	1.0329	3.2576	14615	1.0639	2.9932
Ave.	14879	1.0394	3.0663	14579	1.0380	3.0546	14500	1.0537	3.1224	14039	1.0552	3.0941
SD	213	0.0119	0.1079	114	0.0133	0.1611	327	0.0140	0.1073	347	0.0093	0.0736

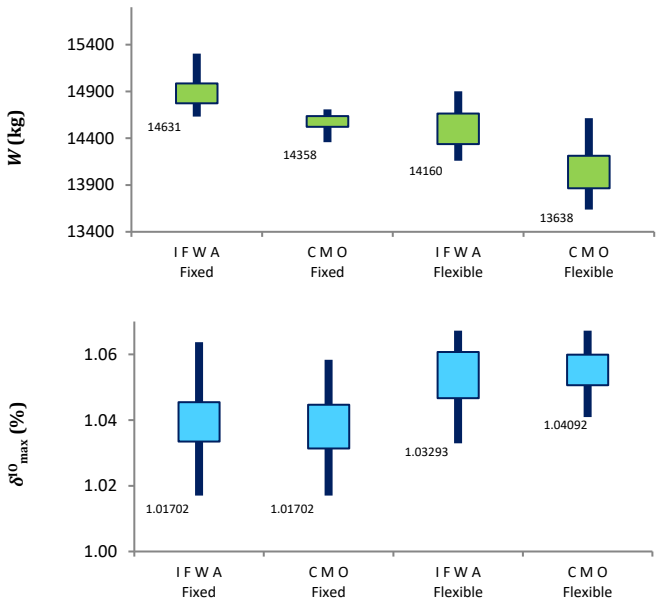

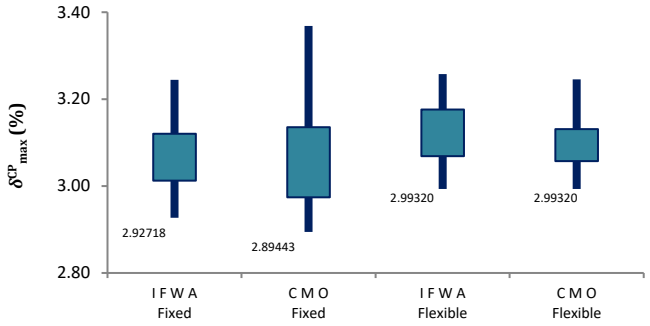

Figure 4. Bar graphs for 6-story MRF

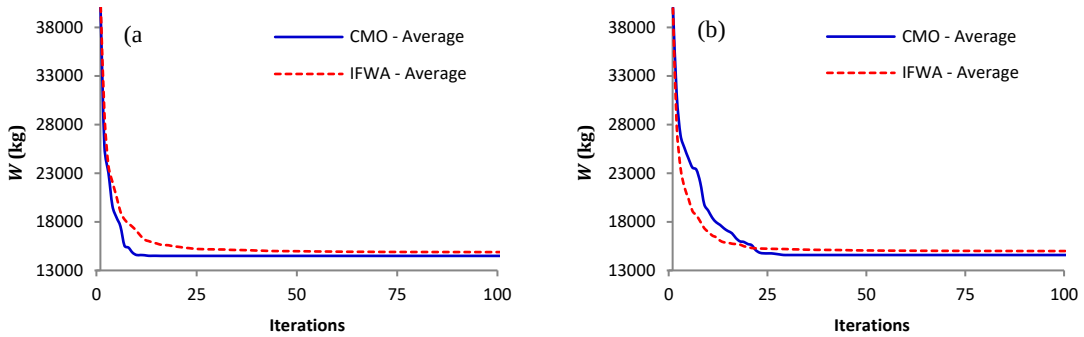

Figure 5. Mean convergence histories for 6-story MRF, a) fixed base b) flexible base models

These results show that the CMO algorithm outperforms IFWA in terms of average optimal weight and convergence rate in both the fixed and flexible base models. The best structural weights found by IFWA and CMO metaheuristics for fixed base model are 14631 and 14358 kg and for flexible base model are 14160 and 13638 kg, respectively. This means that the best optimal design found by CMO considering SSI effects is 5.01% lighter compared to the fixed base model. The results indicate that, the average optimal weight found by CMO for flexible base model is 3.7% lighter than that of the fixed base model.

The inter-story drifts of the best optimal designs and the mean inter-story drifts of all designs found by CMO for both the fixed and flexible base models are respectively shown in Figs. 7 and 8 at IO and CP performance levels. It can be observed that the inter-story drifts along with the height of both the models are almost the same, especially at CP performance level. However, the average δ^{IO}_{max} and δ^{CP}_{max} for the flexible base model is slightly more than those of the fixed base models.

It can be seen from the obtained results that the SD values of the nonlinear structural seismic responses of flexible base model, including δ^{IO}_{max} and δ^{CP}_{max}, are less compared to fixed base model.

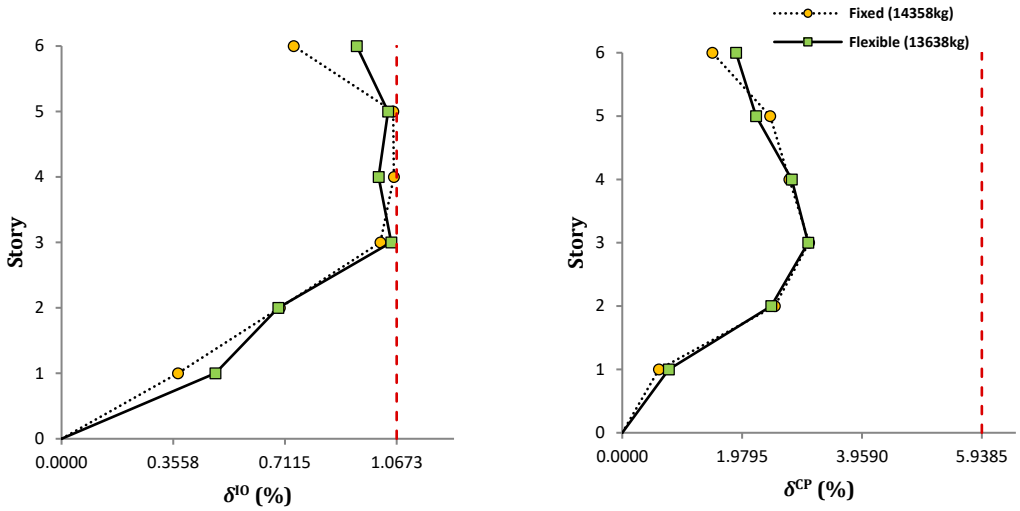

Figure 6. Inter-story drift profiles for the best optimal 6-story MRFs with fixed and flexible bases found by CMO

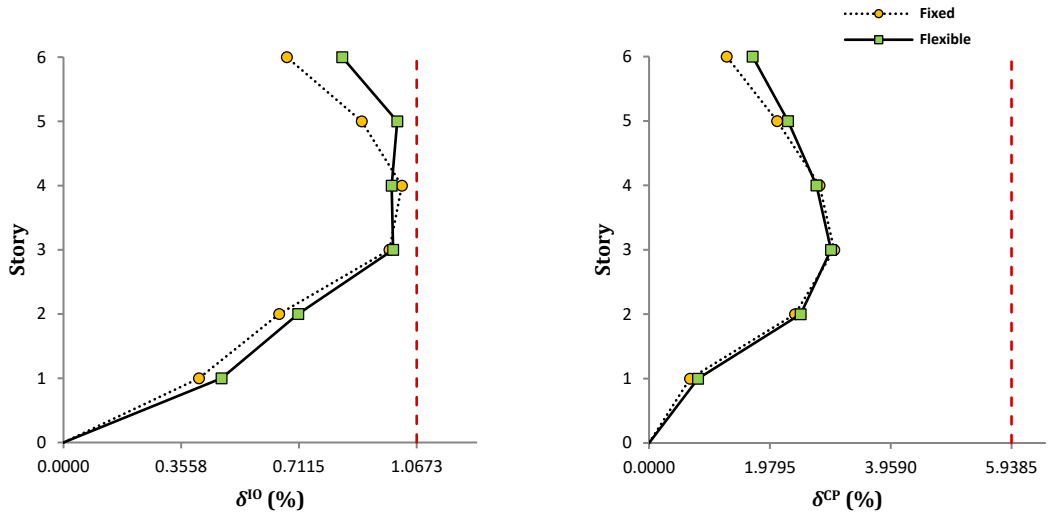

Figure 7. Mean inter-story drift profiles for the optimal 6-story MRFs with fixed and flexible bases found by CMO

5.2 12-story MRF

In SSI modeling of 12-story structures, sandy soil with a unit weight of 18 kN/m^3 is considered, shear wave velocity is 185 m/s, cohesion is 5000 kPa and the friction angle is 38◦. The total length of the foundation is 24 m, the width of the strip is 2.8 m and the height of the foundation is 1.4 m. The parameters R_k, R_e, S_e are 1.54, 0.07, 0.05, respectively.

Table 4. Results of independent optimization runs for fixed and flexible base 12-story MRFs

Design No.	Fixed base						Flexible base					
	IFWA			CMO			IFWA			CMO		
	W (kg)	δ_{max}^{IO} (%)	δ_{max}^{CP} (%)	W (kg)	δ_{max}^{IO} (%)	δ_{max}^{CP} (%)	W (kg)	δ_{max}^{IO} (%)	δ_{max}^{CP} (%)	W (kg)	δ_{max}^{IO} (%)	δ_{max}^{CP} (%)
1	49722	1.0311	3.4130	**48802**	**1.0536**	**4.2306**	48957	1.0501	4.2579	47686	1.0267	4.0716
2	50882	1.0291	3.0159	49839	1.0634	3.3373	48957	1.0501	4.2579	47553	1.0329	4.1907
3	50599	1.0203	4.2726	48802	1.0536	4.2306	47686	1.0267	4.0716	47461	1.0213	3.9867
4	50695	1.0339	4.1761	49700	1.0565	3.4259	48135	1.0488	4.2755	47553	1.0329	4.1907
5	50525	1.0482	4.3123	49700	1.0565	3.4259	48128	1.0278	4.4013	**46332**	**1.0480**	**4.2620**
6	50773	1.0299	3.2924	49722	1.0311	3.4130	**47461**	**1.0213**	**3.9867**	46332	1.0480	4.2620
7	50568	1.0337	4.2227	48802	1.0536	4.2306	47553	1.0329	4.1907	48135	1.0488	4.2755
8	50773	1.0299	3.2924	49289	1.0498	3.4650	47461	1.0213	3.9867	48135	1.0488	4.2755
9	50779	1.0239	4.1308	49205	1.0204	4.3634	47553	1.0329	4.1907	47553	1.0329	4.1907
10	50869	1.0349	4.2067	49700	1.0565	3.4259	47686	1.0267	4.0716	46332	1.0480	4.2620
11	50692	1.0485	4.2401	49341	1.0222	4.4310	48128	1.0278	4.4013	47461	1.0213	3.9867
12	49575	1.0187	4.3944	49837	1.0176	4.1953	47461	1.0213	3.9867	47461	1.0213	3.9867
13	50549	1.0529	4.2415	49173	1.0439	3.0602	49810	1.0412	4.2577	48135	1.0488	4.2755
14	51907	1.0257	3.1095	49239	1.0235	3.5840	49810	1.0412	4.2577	46332	1.0480	4.2620
15	49700	1.0565	3.4259	48832	1.0279	4.1578	48128	1.0278	4.4013	46332	1.0480	4.2620
16	50887	1.0532	4.3480	48802	1.0536	4.2306	48128	1.0278	4.4013	47461	1.0213	3.9867
17	50734	1.0273	3.2785	49835	1.0210	4.4411	47686	1.0267	4.0716	47686	1.0267	4.0716
18	51051	1.0237	4.4483	49625	1.0521	4.4707	48957	1.0501	4.2579	47686	1.0267	4.0716
19	**49205**	**1.0204**	**4.3634**	49575	1.0187	4.3944	47686	1.0267	4.0716	47686	1.0267	4.0716
20	50617	1.0510	4.3718	48802	1.0536	4.2306	47461	1.0213	3.9867	47553	1.0329	4.1907
Ave.	50555	1.0347	3.9278	49331	1.0415	3.9372	48142	1.0325	4.1892	47343	1.0355	4.1566
SD	599	0.0124	0.5145	409	0.0162	0.4732	759	0.0104	0.1504	637	0.0113	0.1140

The number of search agents and the maximum number of iterations are taken as 100 and 100, respectively. Table 4 gives the results of 20 independent PBD optimization runs for 12-story steel MRF. The comparison of the results is done by using bar graphs as represented in Fig. 8. Moreover, mean convergence histories of the metaheuristics are shown in Fig. 9. The results indicate that in both the fixed and flexible base models, the average optimal weight and convergence rate of the CMO are better than those of IFWA. The best structural weights found by IFWA and CMO for fixed base model are 49205 and 48802 kg and for flexible base model are 47461 and 46332 kg, respectively. The best and average optimal weights of the flexible base model is 5.06% and 4.03% lighter than those of the fixed base one.

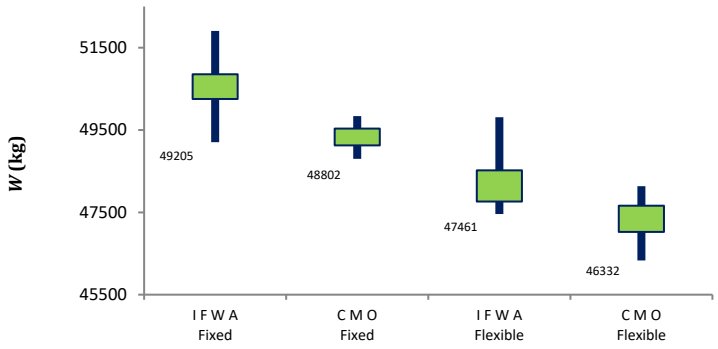

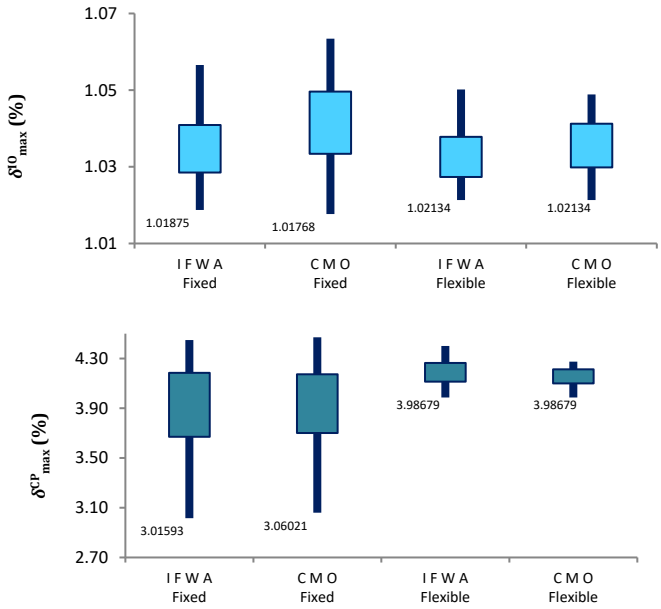

Figure 8. Bar graphs for12-story MRFs

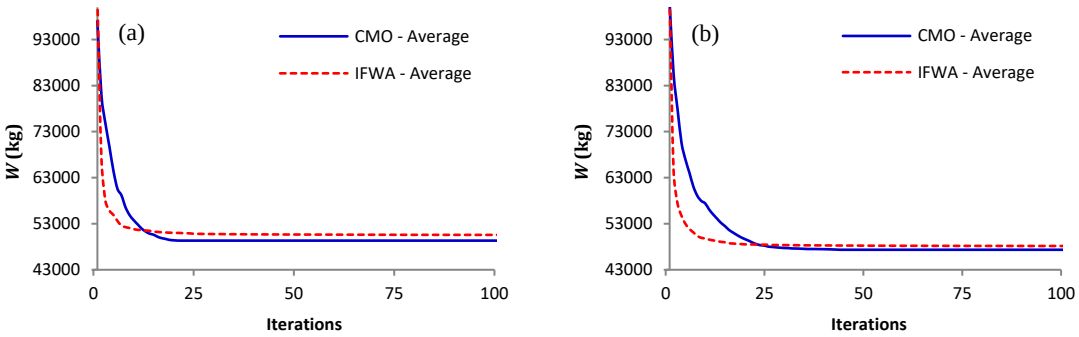

Figure 9. Mean convergence histories for 12-story MRF, a) fixed base b) flexible base models

Figs. 11 and 12 respectively illustrate the inter-story drifts of the best optimal designs and the mean inter-story drifts of all designs, at IO and CP performance levels, found by CMO for both the fixed and flexible base models. It can be seen from Figure 10 that δ^{IO}_{max} and δ^{CP}_{max} for both the models are identical and difference between inter-story drifts in some floors is considerable. Figure 11 indicates that there is a significant difference between inter-story drifts of the models at IO level in most of the floors and the differences in CP level are decreased especially in upper floors.

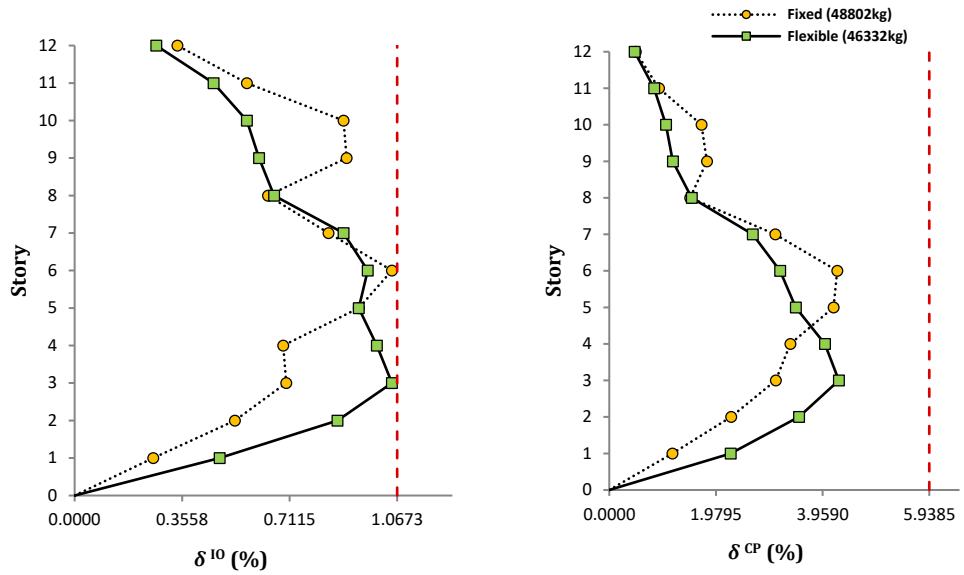

Figure 10. Inter-story drift profiles for the best optimal 12-story MRFs with fixed and flexible bases found by CMO

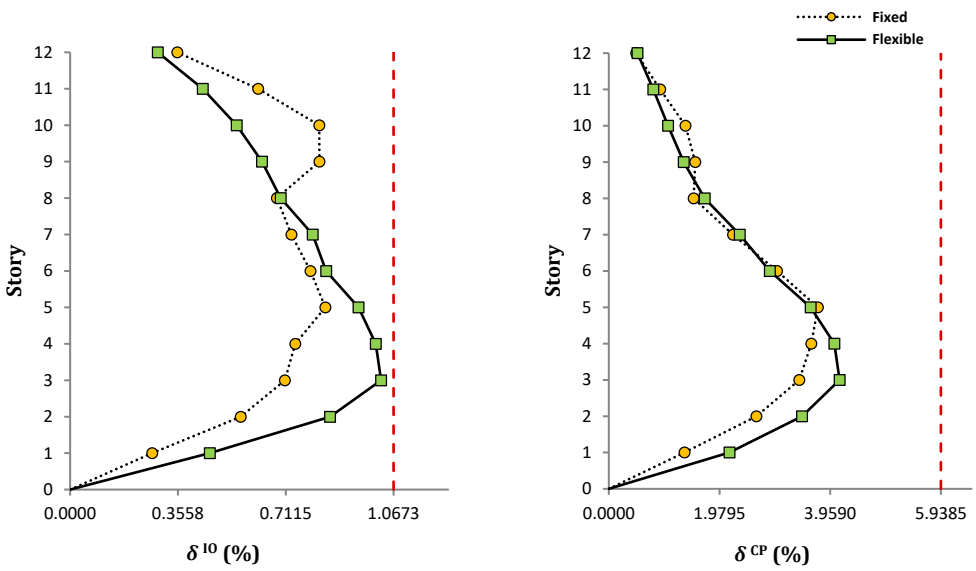

Figure 11. Mean inter-story drift profiles for the optimal 12-story MRFs with fixed and flexible bases found by CMO

For the flexible base model, the average $\delta_{\max}^{\mathrm{CP}}$ is about 6% more than that of the fixed base model while the average $\delta_{\max}^{\mathrm{IO}}$ for both the model is almost the same. For flexible base model of 12-story steel MRF, the SD values of the nonlinear structural responses are less than those of the fixed base one.

6. CONCLUSION

The present study is aimed at performance-based seismic design optimization of steel special moment resisting frame (MRF) structures considering soil-structure interaction. The PBD optimization problem is tackled by center of mass optimization (CMO) and improved fireworks algorithm (IFWA). During the optimization process, nonlinear response history analysis is performed to evaluate the required seismic structural response. Two design examples of 6- and 12-story steel MRFs are presented and for each example two fixed and flexible base models are adopted. For each model, 20 independent optimization runs are implemented in the context of PBD and the optimal designs are compared by taking into account various parameters including structural optimal weight and nonlinear structural responses of inter-story drift at IO and CP levels ($\delta^{\mathrm{IO}}$and δ^{CP}). The following conclusions can be drawn based on the results obtained in this study:

- In both design examples, CMO outperforms IFWA in terms of average optimal weight and convergence rate for both the fixed and flexible base models.
- The soil-structure interaction leads to a reduction in structural optimal weight by a factor of 3.70% for 6-story and 4.03% for 12-story steel MRFs.
- For 6- story steel MRF, the average $\delta_{\max}^{\mathrm{IO}}$ and $\delta_{\max}^{\mathrm{CP}}$ for the flexible base model is slightly more than those of the fixed base models. In the case of 12-story steel MRF, for the flexible base model, the average $\delta_{\max}^{\mathrm{CP}}$ is about 6% more than that of the fixed base model while the average $\delta_{\max}^{\mathrm{IO}}$ for both the model is almost the same.
- The standard deviation of the nonlinear structural seismic responses of flexible base model are less compared to fixed base model.

Finally, it can be concluded that the soil-structure interaction may not be ignored in the design process of steel special moment resisting frames.

6. APPENDIX

In this section, the cross-sections of beams and columns of all the optimal designs are presented based on the available W-shaped steel sections of Table 2.

Table A1: Cross-sections of 20 fixed base optimal 6-story MRFs found by IFWA

Variables	1	2	3	4	5	6	7	8	9	10	11	12	13	14	15	16	17	18	19	20
B1	12	16	15	11	12	16	13	13	13	14	14	16	14	12	14	14	14	16	14	16
B2	12	8	11	13	12	10	8	10	10	9	10	8	9	9	12	10	10	8	9	8
B3	10	16	11	11	10	13	16	12	12	10	10	16	10	12	6	9	10	16	8	16
B4	16	7	12	14	16	16	13	14	14	16	16	7	16	9	18	15	16	7	16	7
B5	15	14	15	12	15	11	16	14	14	13	15	14	13	10	14	14	15	14	11	14
B6	12	12	12	8	12	15	15	12	12	16	9	12	16	11	12	10	9	12	11	12
C1	17	17	17	18	17	17	17	17	17	17	16	17	17	18	17	18	16	17	17	17
C2	17	18	19	18	17	19	18	19	19	18	19	18	18	20	19	19	19	18	19	18
C3	19	19	19	20	19	20	20	20	20	20	20	19	20	20	19	19	20	19	19	19
C4	18	16	17	17	18	16	17	17	17	16	16	16	16	16	17	16	16	16	16	16
C5	18	18	18	17	18	17	17	17	17	17	17	18	17	18	17	16	17	18	17	18
C6	18	19	19	20	18	17	17	17	17	18	17	19	18	19	17	17	17	19	18	19

Table A2: Cross-sections of 20 fixed base optimal 6-story MRFs found by CMO

Variables	1	2	3	4	5	6	7	8	9	10	11	12	13	14	15	16	17	18	19	20
B1	12	15	12	14	16	15	12	16	12	12	16	16	16	16	16	15	14	15	16	16
B2	9	8	9	9	8	8	9	8	9	9	8	8	8	8	8	8	9	8	8	8
B3	13	12	12	10	16	12	13	16	12	12	16	16	16	16	16	12	10	12	16	16
B4	16	8	9	16	14	16	16	7	9	9	7	7	7	7	7	16	16	8	7	7
B5	13	15	10	13	10	15	13	14	10	10	14	14	14	14	14	15	13	15	14	14
B6	18	14	11	16	12	13	18	12	11	11	12	12	12	12	12	13	16	14	12	12
C1	18	18	18	17	18	18	18	17	18	18	17	17	17	17	17	18	17	18	17	17
C2	19	20	20	18	18	18	19	18	20	20	18	18	18	18	18	18	18	20	18	18
C3	20	20	20	20	18	18	20	19	20	20	19	19	19	19	19	18	20	20	19	19
C4	17	18	16	16	18	18	17	16	16	16	16	16	16	16	16	18	16	18	16	16
C5	17	18	18	17	18	19	17	18	18	18	18	18	18	18	18	19	17	18	18	18
C6	17	18	19	18	19	19	17	19	19	19	19	19	19	19	19	19	18	18	19	19

Table A3: Cross-sections of 20 flexible base optimal 6-story MRFs found by IFWA

Variables	1	2	3	4	5	6	7	8	9	10	11	12	13	14	15	16	17	18	19	20
B1	9	9	9	9	9	9	9	16	16	9	16	9	16	9	9	9	16	9	16	16
B2	5	11	11	5	11	5	11	8	8	5	8	11	8	11	11	5	8	11	8	8
B3	15	13	13	15	13	15	13	14	14	15	14	13	14	13	13	15	14	13	8	14
B4	13	16	16	13	16	13	16	14	14	13	14	16	14	16	16	13	14	16	9	14
B5	10	9	9	10	9	10	9	15	15	10	15	9	15	9	9	10	15	9	8	15
B6	14	18	18	14	18	14	18	11	11	14	11	18	11	18	18	14	11	18	13	11
C1	18	19	19	18	19	18	19	18	18	18	18	19	18	19	19	18	18	19	17	18
C2	19	19	19	19	19	19	19	18	18	19	18	19	18	19	19	19	18	19	19	18
C3	19	19	19	19	19	19	19	18	18	19	18	19	18	19	19	19	18	19	19	18
C4	18	17	17	18	17	18	17	17	17	18	17	17	17	17	17	18	17	17	18	17
C5	19	18	18	19	18	19	18	17	17	19	17	18	17	18	18	19	17	18	19	17
C6	19	18	18	19	18	19	18	19	19	19	19	18	19	18	18	19	19	18	19	19

Table A4: Cross-sections of 20 flexible base optimal 6-story MRFs found by CMO

Variables	1	2	3	4	5	6	7	8	9	10	11	12	13	14	15	16	17	18	19	20
B1	18	16	16	18	18	9	16	9	18	16	16	16	16	16	16	9	9	16	9	9
B2	7	15	15	7	7	5	15	11	7	15	8	8	15	15	15	5	11	8	11	5
B3	8	7	7	8	8	15	7	13	8	7	8	8	7	7	7	15	13	8	13	15
B4	18	18	18	18	18	13	18	16	18	18	9	9	18	18	18	13	16	9	16	13
B5	9	11	11	9	9	10	11	9	9	11	8	8	11	11	11	10	9	8	9	10
B6	16	14	14	16	16	14	14	18	16	14	13	13	14	14	14	14	18	13	18	14
C1	16	19	19	16	16	18	19	19	16	19	17	17	19	19	19	18	19	17	19	18
C2	17	19	19	17	17	19	19	19	17	19	19	19	19	19	19	19	19	19	19	19
C3	20	20	20	20	20	19	20	19	20	20	19	19	20	20	20	19	19	19	19	19
C4	18	16	16	18	18	18	16	17	18	16	18	18	16	16	16	18	17	18	17	18
C5	19	19	19	19	19	19	19	18	19	19	19	19	19	19	19	19	18	19	18	19
C6	19	20	20	19	19	19	20	18	19	20	19	19	20	20	20	19	18	19	18	19

Table A5: Cross-sections of 20 fixed base optimal 12-story MRFs found by IFWA

Variables	1	2	3	4	5	6	7	8	9	10	11	12	13	14	15	16	17	18	19	20
B1	8	9	5	7	6	10	7	10	5	8	6	3	7	9	9	7	8	2	4	8
B2	5	8	14	11	14	9	14	9	14	15	14	15	10	10	9	14	9	15	14	15
B3	5	6	9	15	11	4	9	4	9	10	10	9	15	7	6	10	4	10	8	14
B4	11	11	10	8	10	11	7	11	8	8	8	9	7	5	12	9	11	9	9	8
B5	7	5	12	13	12	4	13	4	12	10	11	12	14	10	6	10	5	12	12	12
B6	9	7	6	13	6	7	6	7	6	7	5	8	12	10	7	7	4	5	7	9
B7	6	12	7	7	6	11	5	11	6	7	6	6	6	8	12	7	13	7	6	7
B8	15	8	8	9	7	8	5	8	6	6	8	9	8	10	7	8	7	8	9	8
B9	5	11	9	10	9	11	6	11	9	9	9	9	5	9	11	6	11	10	8	13
B10	7	11	7	8	8	11	8	11	6	5	7	7	8	9	11	9	11	7	7	6
B11	7	8	11	9	13	9	13	9	11	11	11	11	9	11	9	11	9	11	11	10

Variables	1	2	3	4	5	6	7	8	9	10	11	12	13	14	15	16	17	18	19	20
B12	11	4	9	8	7	5	9	5	10	9	7	9	8	13	4	9	5	9	10	8
C1	13	14	12	13	12	13	12	13	12	12	12	12	13	14	13	12	13	12	12	13
C2	15	14	13	14	14	14	14	14	13	13	14	13	14	14	14	13	14	14	14	13
C3	16	17	17	15	17	17	17	17	17	16	17	17	14	15	17	17	16	16	17	14
C4	17	18	17	15	17	18	17	18	17	17	17	17	15	16	18	17	18	17	17	15
C5	17	19	17	18	17	19	17	19	17	17	17	17	18	16	19	17	19	17	17	17
C6	17	20	18	20	18	20	18	20	19	18	18	17	20	17	20	17	19	18	18	19
C7	12	12	14	12	14	13	14	13	14	14	14	14	12	13	13	14	13	14	14	13
C8	16	14	14	14	14	13	15	13	14	14	14	14	15	13	14	14	15	14	14	13
C9	17	14	15	16	16	14	16	14	15	14	16	16	16	14	14	14	15	16	17	16
C10	17	15	17	18	17	15	17	15	17	16	17	17	18	15	15	17	15	17	17	18
C11	19	16	17	18	17	16	17	16	17	17	17	17	18	19	16	17	16	17	17	18
C12	19	19	18	19	18	20	19	20	19	19	18	18	19	19	20	19	19	18	18	19
C13	13	13	14	14	13	13	14	13	13	14	14	14	14	14	12	13	13	13	14	14
C14	14	15	14	15	14	16	14	16	13	14	14	14	15	15	15	13	16	14	14	15
C15	14	17	14	16	14	17	14	17	14	14	14	14	16	16	17	14	17	14	14	16
C16	16	17	16	17	15	17	17	17	17	17	14	16	17	16	17	17	17	16	16	17
C17	17	17	18	19	18	17	17	17	19	19	18	18	19	16	17	19	17	18	19	18
C18	18	17	19	20	19	17	20	17	19	20	20	19	19	18	17	20	17	19	19	19

Table A6: Cross-sections of 20 fixed base optimal 12-story MRFs found by CMO

Variables	1	2	3	4	5	6	7	8	9	10	11	12	13	14	15	16	17	18	19	20
B1	8	8	8	9	9	8	8	9	4	9	6	3	9	9	6	8	2	6	3	8
B2	9	9	9	9	9	5	9	10	14	9	14	13	9	9	10	9	7	14	15	9
B3	15	6	15	6	6	5	15	6	8	6	9	12	3	7	10	15	14	9	9	15
B4	6	12	6	12	12	11	6	12	9	12	9	11	12	10	9	6	8	11	9	6
B5	14	6	14	6	6	7	14	7	12	6	12	9	3	10	8	14	12	11	12	14
B6	12	7	12	7	7	9	12	6	7	7	6	9	8	8	9	12	7	6	8	12
B7	7	12	7	12	12	6	7	11	6	12	6	10	10	10	10	7	8	6	6	7
B8	6	7	6	7	7	15	6	8	9	7	8	12	8	7	11	6	12	8	9	6
B9	13	11	13	11	11	5	13	11	8	11	9	5	11	8	6	13	3	9	9	13
B10	7	11	7	11	11	7	7	11	7	11	6	9	9	13	5	7	6	7	7	7
B11	10	9	10	9	9	7	10	7	11	9	11	5	9	11	4	10	11	11	11	10
B12	9	4	9	4	4	11	9	5	10	4	9	10	4	6	7	9	9	9	9	9
C1	12	13	12	13	13	13	12	14	12	13	12	13	13	14	13	12	14	12	12	12
C2	14	14	14	14	14	15	14	15	14	14	14	14	15	15	14	14	15	13	13	14
C3	15	17	15	17	17	16	15	16	17	17	16	16	17	16	16	15	17	17	17	15
C4	16	18	16	18	18	17	16	18	17	18	17	17	18	18	16	16	19	17	17	16
C5	18	19	18	19	19	17	18	18	17	19	17	17	19	19	17	18	19	17	17	18
C6	20	20	20	20	20	17	20	20	18	20	18	18	20	19	17	20	20	18	17	20
C7	12	13	12	13	13	12	12	13	14	13	14	15	13	13	15	12	14	13	14	12
C8	13	14	13	14	14	16	13	13	14	14	14	15	14	14	16	13	14	15	14	13
C9	18	14	18	14	14	17	18	14	17	14	16	16	14	15	17	18	16	16	16	18
C10	18	15	18	15	15	17	18	16	17	15	16	18	16	15	18	18	16	17	17	18
C11	18	16	18	16	16	19	18	17	17	16	17	18	16	16	18	18	16	17	17	18
C12	19	19	19	20	20	19	19	17	18	20	18	19	19	19	18	19	18	19	18	19
C13	14	13	14	12	12	13	14	13	14	12	13	14	13	13	14	14	14	13	14	14
C14	15	15	15	15	15	14	15	16	14	15	14	14	16	17	14	15	14	14	14	15
C15	16	17	16	17	17	14	16	17	14	17	15	15	17	17	14	16	14	14	14	16
C16	17	17	17	17	17	16	17	17	16	17	16	15	17	17	16	17	15	16	16	17
C17	19	17	19	17	17	17	19	18	19	17	18	16	18	17	16	19	16	18	18	19
C18	19	17	19	17	17	18	19	18	19	17	19	17	18	18	18	19	18	19	19	19

Table A7: Cross-sections of 20 flexible base optimal 12-story MRFs found by IFWA

Variables	1	2	3	4	5	6	7	8	9	10	11	12	13	14	15	16	17	18	19	20
B1	11	11	9	9	13	4	9	9	9	9	13	4	10	10	13	13	9	11	9	9
B2	13	13	11	12	13	15	13	9	13	11	13	15	13	13	13	13	11	13	11	9
B3	8	8	9	9	10	12	9	8	9	9	10	12	8	8	10	10	9	8	9	8
B4	9	9	10	11	10	3	9	11	9	10	10	3	10	10	10	10	10	9	10	11
B5	10	10	9	9	9	11	9	8	9	9	9	11	7	7	9	9	9	10	9	8
B6	9	9	6	8	8	8	9	10	9	6	8	8	10	10	8	8	6	9	6	10
B7	12	12	12	12	11	4	12	9	12	12	11	4	7	7	11	11	12	12	12	9
B8	8	8	10	10	9	10	9	9	9	10	9	10	8	8	9	9	10	8	10	9
B9	10	10	9	11	12	8	10	6	10	9	12	8	11	11	12	12	9	10	9	6
B10	4	4	8	8	10	8	7	7	7	8	10	8	6	6	10	10	8	4	8	7
B11	8	8	11	11	10	9	11	9	11	11	10	9	6	6	10	10	11	8	11	9
B12	9	9	11	11	11	8	11	6	11	11	11	8	7	7	11	11	11	9	11	6
C1	14	14	15	15	15	14	15	15	15	15	15	14	15	15	15	15	15	14	15	15
C2	14	14	16	16	16	15	16	16	16	16	16	15	15	15	16	16	16	14	16	16
C3	15	15	16	16	16	16	16	17	16	16	16	16	15	15	16	16	16	15	16	17
C4	15	15	16	16	16	17	16	17	16	16	16	17	15	15	16	16	16	15	16	17
C5	16	16	16	16	16	18	16	18	16	16	16	18	16	16	16	16	16	16	16	18
C6	16	16	18	18	18	18	18	18	18	18	18	18	16	16	18	18	18	16	18	18
C7	13	13	14	14	14	13	14	13	14	14	14	13	14	14	14	14	14	13	14	13
C8	17	17	14	14	14	13	14	13	14	14	14	13	16	16	14	14	14	17	14	13
C9	18	18	16	15	16	16	15	16	15	16	16	16	18	18	16	16	16	18	16	16
C10	18	18	16	16	17	16	16	16	16	16	17	16	18	18	17	17	16	18	16	16
C11	19	19	17	17	17	17	17	17	17	17	17	17	19	19	17	17	17	19	17	17
C12	19	19	18	18	18	19	18	19	18	18	18	19	19	19	18	18	18	19	18	19
C13	14	14	13	13	13	12	13	12	13	13	13	12	14	14	13	13	13	14	13	12
C14	14	14	13	13	13	16	13	16	13	13	13	16	14	14	13	13	13	14	13	16
C15	15	15	13	13	13	16	13	16	13	13	13	16	14	14	13	13	13	15	13	16
C16	16	16	16	16	16	16	16	16	16	16	16	16	16	16	16	16	16	16	16	16
C17	19	19	16	16	17	16	17	16	17	16	17	16	19	19	17	17	16	19	16	16
C18	19	19	19	19	20	17	19	17	19	19	20	17	19	19	20	20	19	19	19	17

Table A8: Cross-sections of 20 flexible base optimal 12-story MRFs found by CMO

Variables	1	2	3	4	5	6	7	8	9	10	11	12	13	14	15	16	17	18	19	20
B1	9	9	9	9	12	12	9	9	9	12	9	9	9	12	12	9	9	9	9	9
B2	11	13	9	13	10	10	12	12	13	10	9	9	12	10	10	9	11	11	11	13
B3	9	9	8	9	8	8	9	9	9	8	8	8	9	8	8	8	9	9	9	9
B4	10	9	11	9	8	8	11	11	9	8	11	11	11	8	8	11	10	10	10	9
B5	9	9	8	9	8	8	9	9	9	8	8	8	9	8	8	8	9	9	9	9
B6	6	9	10	9	14	14	8	8	9	14	10	10	8	14	14	10	6	6	6	9
B7	12	12	9	12	8	8	12	12	12	8	9	9	12	8	8	9	12	12	12	12
B8	10	9	9	9	8	8	10	10	9	8	9	9	10	8	8	9	10	10	10	9
B9	9	10	6	10	8	8	11	11	10	8	6	6	11	8	8	6	9	9	9	10
B10	8	7	7	7	11	11	8	8	7	11	7	7	8	11	11	7	8	8	8	7
B11	11	11	9	11	8	8	11	11	11	8	9	9	11	8	8	9	11	11	11	11
B12	11	11	6	11	8	8	11	11	11	8	6	6	11	8	8	6	11	11	11	11
C1	15	15	15	15	14	14	15	15	15	14	15	15	15	14	14	15	15	15	15	15
C2	16	16	16	16	15	15	16	16	16	15	16	16	16	15	15	16	16	16	16	16
C3	16	16	17	16	15	15	16	16	16	15	17	17	16	15	15	17	16	16	16	16
C4	16	16	17	16	16	16	16	16	16	16	17	17	16	16	16	17	16	16	16	16
C5	16	16	18	16	19	19	16	16	16	19	18	18	16	19	19	18	16	16	16	16
C6	18	18	18	18	19	19	18	18	18	19	18	18	18	19	19	18	18	18	18	18
C7	14	14	13	14	15	15	14	14	14	15	13	13	14	15	15	13	14	14	14	14
C8	14	14	13	14	16	16	14	14	14	16	13	13	14	16	16	13	14	14	14	14
C9	16	15	16	15	16	16	15	15	15	16	16	16	15	16	16	16	16	16	16	15
C10	16	16	16	16	17	17	16	16	16	17	16	16	16	17	17	16	16	16	16	16
C11	17	17	17	17	17	17	17	17	17	17	17	17	17	17	17	17	17	17	17	17
C12	18	18	19	18	19	19	18	18	18	19	19	19	18	19	19	19	18	18	18	18
C13	13	13	12	13	12	12	13	13	13	12	12	12	13	12	12	12	13	13	13	13
C14	13	13	16	13	16	16	13	13	13	16	16	16	13	16	16	16	13	13	13	13
C15	13	13	16	13	17	17	13	13	13	17	16	16	13	17	17	16	13	13	13	13
C16	16	16	16	16	17	17	16	16	16	17	16	16	16	17	17	16	16	16	16	16

Variables	1	2	3	4	5	6	7	8	9	10	11	12	13	14	15	16	17	18	19	20
C17	16	17	16	17	17	17	16	16	17	17	16	16	16	17	17	16	16	16	16	17
C18	19	19	17	19	19	19	19	19	19	19	17	17	19	19	19	17	19	19	19	19

REFERENCES

1. Ghannad MA, Jahankhah H. Site-dependent strength reduction factors for soil-structure systems, *Soil Dyn Earthq Eng* 2007; **27**:99-110.
2. Mylonakis G, Gazetas G. Seismic soil-structure interaction: beneficial or detrimental?, *J Earthq Eng* 2000; **4**: 277-301.
3. Liu M, Wen YK, Burns SA. Life cycle cost oriented seismic design optimization of steel moment frame structures with risk-taking preference, *Eng Struct* 2004; **26**: 1407-21.
4. Fragiadakis M, Lagaros ND, Papadrakakis M. Performance-based multiobjective optimum design of steel structures considering life-cycle cost, *Struct Multidis Optim* 2006; **32**: 1.
5. Rojas HA, Pezeshk S, Foley CM. Performance-based optimization considering both structural and nonstructural components, *Earthqu Spectra* 2007; **23**: 685-709.
6. Lagaros ND, Fragiadakis M. Robust performance-based design optimization of steel moment resisting frames, *J Earthq Eng* 2007; **11**: 752-72.
7. Möller O, Foschi RO, Quiroz LM, Rubinstein M. Structural optimization for performance-based design in earthquake engineering: applications of neural networks, *Struct Safe* 2009; **31**: 490-9.
8. Ghosh S, Datta D, Katakdhond AA. Estimation of the Park–Ang damage index for planar multi-storey frames using equivalent single-degree systems, *Eng Struct* 2011; **33**: 2509-24.
9. Kaveh A, Nasrollahi A. Performance-based seismic design of steel frames utilizing charged system search optimization, *Appl Soft Comput* 2014; **22**: 213-21.
10. Sanaz Saadat, Charles V. Camp, Pezeshk S. Seismic performance-based design optimization considering direct economic loss and direct social loss, *Eng Struct* 2014; **79**: 193-201.
11. Gholizadeh S, Milany A. Optimal performance-based design of steel frames using advanced metaheuristics, *Asian J Civil Eng* 2016; **17**: 607-23.
12. Gholizadeh S, Fattahi F. Damage-controlled performance-based design optimization of steel moment frames, *Struct Des Tall Special Build* 2018; **27**: e1498.
13. Fattahi F, Gholizadeh S. Seismic fragility assessment of optimally designed steel moment frames, *Eng Struct* 2019; **179**: 37-51.
14. Steneker P, Filiatrault A, Wiebe L, Konstantinidis D. Integrated structural-nonstructural performance-based seismic design and retrofit optimization of buildings, *J Struct Eng* 2020; **146**: 04020141.
15. Degertekin SO, Tutar H, Lamberti L. School-based optimization for performance-based optimum seismic design of steel frames, *Eng Comput* 2020.
16. Idels O, Lavan O. Performance based formal optimized seismic design of steel moment resisting frames, *Comput Struct* 2020; **235**: 106269.

17. Ahmadie Amiri H, Pournamazian Najafabadi E, Esmailpur Estekanchi H, Ozbakkaloglu T. Performance-based seismic design and assessment of low-rise steel special moment resisting frames with block slit dampers using endurance time method, *Eng Struct* 2020; **224**: 110955.
18. Montuori R, Nastri E, Piluso V, Todisco P. A simplified performance based approach for the evaluation of seismic performances of steel frames, *Eng Struct* 2020; **224**: 111222.
19. Nakhaei M, Ghannad MA. The effect of soil–structure interaction on damage index of buildings, *Eng Struct* 2008; **30**: 1491-9.
20. Sáez E, Lopez-Caballero F, Modaressi-Farahmand-Razavi A. Effect of the inelastic dynamic soil–structure interaction on the seismic vulnerability assessment, *Struct Safe* 2011; **33**: 51-63.
21. Raychowdhury P. Seismic response of low-rise steel moment-resisting frame (SMRF) buildings incorporating nonlinear soil–structure interaction (SSI), *Eng Struct* 2011; **33**: 958-67.
22. Ganjavi B, Hao H. A parametric study on the evaluation of ductility demand distribution in multi-degree-of-freedom systems considering soil–structure interaction effects, *Eng Struct* 2012; **43**: 88-104.
23. Sáez E, Lopez-Caballero F, Modaressi-Farahmand-Razavi A. Inelastic dynamic soil-structure interaction effects on moment-resisting frame buildings, *Eng Struct* 2013; **51**: 166-77.
24. Raychowdhury P, Ray-Chaudhuri S. Seismic response of nonstructural components supported by a 4-story SMRF: Effect of nonlinear soil–structure interaction, *Struct* 2015; **3**: 200-10.
25. Lu Y, Hajirasouliha I, Marshall AM. Performance-based seismic design of flexible-base multi-storey buildings considering soil–structure interaction, *Eng Struct* 2016; **108**: 90-103.
26. Aydemir ME, Ekiz I. Soil–structure interaction effects on seismic behaviour of multistorey structures, *European J Environ Civil Eng* 2013; **17**: 635–53.
27. Ghandil M, Behnamfar F. Ductility demands of MRF structures on soft soils considering soil-structure interaction, *Soil Dyn Earthq Eng* 2017; **92**: 203-14.
28. Farhadi N, Saffari H, Torkzadeh P. Estimation of maximum and residual inter-storey drift in steel MRF considering soil-structure interaction from fixed-base analyses, *Soil Dyn Earthq Eng* 2018; **114**: 85-96.
29. Ganjavi B, Gholamrezatabar A, Hajirasouliha I. Effects of soil-structure interaction and lateral design load pattern on performance-based plastic design of steel moment resisting frames, *Struct Des Tall Spec Build* 2019; **28**: e1624.
30. Mashhadi S, Asadi A, Homaei F, Tajammolian H. The performance-based seismic response of special steel MRF: Effects of pulse-like ground motion and foundation safety factor, *Struct* 2020; **28**: 127-40.
31. Jafarieh AH, Ghannad MA. Seismic performance of nonlinear soil-structure systems located on soft soil considering foundation uplifting and soil yielding, *Struct* 2020; **28**: 973-82.

32. Fathizadeh SF, Vosoughi AR, Banan MR. Considering soil–structure interaction effects on performance-based design optimization of moment-resisting steel frames by an engineered cluster-based genetic algorithm, *Eng Optim* 2021; **53**: 440-60.
33. Gholizadeh S, Ebadijalal M. Performance based discrete topology optimization of steel braced frames by a new metaheuristic, *Adv Eng Softw* 2018; **123**: 77-92.
34. Gholizadeh S, Milany A. An improved fireworks algorithm for discrete sizing optimization of steel skeletal structures, *Eng Optim* 2018; **50**: 1829-49.
35. Gholizadeh S, Hassanzadeh A, Milany A, Ghatte HF. On the seismic collapse capacity of optimally designed steel braced frames, *Eng Comput* 2020.
36. FEMA P695 (ATC-63): Quantification of Building Seismic Performance Factors, Appl Tech Council (ATC), 2009.
37. Seismic Evaluation and Retrofit of Existing Buildings, ASCE/SEI 41-13: American Society of Civil Engineers (ASCE), 2013.
38. Raychowdhury P, Hutchinson TC. Performance evaluation of a nonlinear Winkler-based shallow foundation model using centrifuge test results, *Earthq Eng Struct Dyn* 2009; **38**: 679-98.
39. Raychowdhury P. Nonlinear Winkler-based shallow foundation model for performance assessment of seismically loaded structures, UC San Diego Electronic Theses and Dissertations: UC San Diego, 2008.
40. Rajeev P, Tesfamariam S. Seismic fragilities of non-ductile reinforced concrete frames with consideration of soil structure interaction, *Soil Dyn Earthq Eng* 2012; **40**: 78-86.
41. Marzban S, Banazadeh M, Azarbakht A. Seismic performance of reinforced concrete shear wall frames considering soil–foundation–structure interaction, *Struct Des Tall Spec Build* 2014; **23**: 302-18.
42. Shakib H, Homaei F. Probabilistic seismic performance assessment of the soil-structure interaction effect on seismic response of mid-rise setback steel buildings, *Bull Earthq Eng* 2017; **15**: 2827-51.
43. Raychowdhury P, Hutchinson TC. ShallowFoundationGen OpenSees Documentation. Open System for Earthquake Engineering Simulation (OpenSEES): University of California, San Diego, 2008.
44. Boulanger RW, Curras CJ, Kutter BL, Wilson DW, Abghari A. Seismic soil-pile-structure interaction experiments and analyses, *J Geotech Geoenviron Eng* 1999; **125**: 750-9.
45. AISC 360-16: Specification for structural steel buildings, American Institute of Steel Construction (AISC), 2016.
46. FEMA-350: Recommended Seismic Design Criteria for New Steel Moment-Frame Buildings, Federal Emergency Management Agency (FEMA), 2000.